Available online at BCREC website: https://bcrec.id

Bulletin of Chemical Reaction Engineering & Catalysis, 16 (4) 2021, 707-715

Research Article

The Surface Modification of Ag_3PO_4 using Tetrachloroaurate(III) and Metallic Au for Enhanced Photocatalytic Activity

Uyi Sulaeman[1,*], Richo Dwi Permadi[1], Alfa Marcorius[1], Hartiwi Diastuti[1], Anung Riapanitra[1], Shu Yin[2]

[1]*Department of Chemistry, Jenderal Soedirman University, Purwokerto, 53123, Indonesia.*
[2]*Institute of Multidisciplinary Research for Advanced Materials, Tohoku University, Sendai, 980-8577, Japan.*

Received: 20th April 2021; Revised: 30th July 2021; Accepted: 30th July 2021
Available online: 13rd August 2021; Published regularly: December 2021

Abstract

The improvement of Ag_3PO_4 photocatalytic activity was successful by incorporating tetrachloroaurate(III) ($AuCl_4^-$) and metallic Au on the surface of Ag_3PO_4. The photocatalysts were synthesized using the coprecipitation and chemisorption method. Coprecipitation of Ag_3PO_4 was carried out under ethanol-water solution using the starting material of $AgNO_3$ and $Na_2HPO_4.12H_2O$. $AuCl_4^-$ ion and metallic Au were incorporated on the surface of Ag_3PO_4 using a chemisorption method under auric acid solution. The photocatalysts were characterized using XRD, DRS, SEM, and XPS. The $AuCl_4^-$ ion and metallic Au were simultaneously incorporated on the Ag_3PO_4 surface. The high photocatalytic activity might be caused by increasing the separation of hole and electron due to capturing photo-generated electrons by metallic Au and Au(III) as electron acceptors.

Keywords: Chemisorption; Metallic Au; Photocatalyst; Silver Phosphate; Tetrachloroaurate(III)

How to Cite: U. Sulaeman, R.D. Permadi, A. Marcorius, H. Diastuti, A. Riapanitra, S. Yin (2021). The Surface Modification of Ag_3PO_4 using Tetrachloroaurate(III) and Metallic Au for Enhanced Photocatalytic Activity. *Bulletin of Chemical Reaction Engineering & Catalysis*, 16(4), 707-715 (doi: 10.9767/bcrec.16.4.10863.707-715)

Permalink/DOI: https://doi.org/10.9767/bcrec.16.4.10863.707-715

1. Introduction

Recently, the Au dopant-modified photocatalysts have a tremendous great attention for improving the photocatalytic properties. The photocatalyst of Au/TiO_2 [1–3], Au/ZnO [4,5], Au/WO_3 [6], $Au/SrTiO_3$ [7], $Au/g\text{-}C_3N_4$ [8], Au/CdS [9] has been successfully designed for improvement the photocatalytic properties. The incorporation of Au in TiO_2 can reduce Ti^{4+} to Ti^{3+} that effectively enhances the stability and activity [3]. This design also generates a strong plasmon resonance absorption and improves photocatalytic activities. The metallic and ionic Au can be incorporated on the surface of TiO_2. The metallic Au can produce the highest Schottky barrier which facilitates the electron capture, whereas the ionic Au (Au^+ and Au^{3+}) can facilitate electron transfer [10]. Both metallic and ionic Au dopants in TiO_2 inhibit the recombination of electron and hole pairs. The Schottky barrier in the interfacial of metal-ZnO can also be formed by Au, this mechanism can enhance the separation of photogenerated carriers at the ZnO surface [11]. Schottky barriers can increase photoreaction through trapping and prolonging the life of the electrons [12]. However, these

* Corresponding Author.
Email: sulaeman@unsoed.ac.id (U. Sulaeman)

modifications have still drawbacks of photogenerated electron and holes recombination. Therefore, many researchers have developed the synthesis into a multi-component design such as a ternary composite of Au dopant in a photocatalyst.

The ternary composite of Au dopant, such as Au-$CoFe_2O_4/MoS_2$ [13], g-C_3N_4/Au/$ZnIn_2S_4$ [14], rGO/$NiWO_4$@Au [15], Au/CuO/Co_3O_4 [16], and Au/TiO_2@CNTs [17], have been successfully synthesized. The Au has a significant role in the improvement of photocatalytic in these composites. The Au in the Au-$CoFe_2O_4/MoS_2$ and g-C_3N_4/Au/$ZnIn_2S_4$ can effectively act as a facilitator of the Z-scheme mechanism [13,14]. This mechanism maximizes the reaction in the valence band and conduction band, hence improving the photocatalytic activity. The electrons on the surface of Au in the composite of rGO/$NiWO_4$@Au can also act as electron donors, increase the electron transfer and the quantum efficiency leading to high catalytic activity [15]. The Au in Au/CuO/Co_3O_4 effectively mediates an electron trapping that improves the O_2 generation [16]. Plasmonic resonance, the powerful properties of metallic Au, can also be designed in Au/TiO_2@CNTs [17]. This plasmon can have a synergetic effect with CNTs that enhances the transport rates of electrons and holes. However, these multi-components of Au-based photocatalysts have still produced a low quantum efficiency. Therefore, an alternative photocatalyst should be expected.

Ag_3PO_4 is a new photocatalyst that has high quantum efficiency and narrow bandgap energy [18], could be promising as a highly active photocatalyst. Many researchers have focused on modifying this catalyst to improve its properties. The surface modification of the Ag_3PO_4 using Au has been reported [19–21]. Au in the Ag_3PO_4 inhibited the recombination of photogenerated electrons and holes and decreased the photo-corrosion of the Ag_3PO_4 [19]. The Au-incorporated Ag_3PO_4 heterostructure showed highly productive photocatalytic activities [20]. These properties might be induced by the double effect of plasmonic Au nanoparticles and Ag_3PO_4 photoexcitation that generate converting hydroxyl groups into hydroxyl radicals [20]. The Au nanoparticle incorporated on Ag_3PO_4/TiO_2 heterojunctions showed an excellent activity of 10.2 times higher improvement [21]. Based on the literature reports above, both metallic Au and ionic Au have been shown to increase photocatalytic activity. Therefore, it is promising to modify the surface of Ag_3PO_4 using the mixed Au states of metallic Au and ionic Au.

Besides the incorporation of Au on the surface of Ag_3PO_4, the defect formation on Ag_3PO_4 can enhance the photocatalytic properties. The defect sites on Ag_3PO_4 can be initiated under ethanol-water coprecipitation [22]. These defects lead to enhance absorption in the visible region resulting in high photocatalytic activity. A combination of this preparation with Au incorporating might improve the photocatalytic activity significantly.

Herein, the incorporation of $AuCl_4^-$ and metallic Au on the surface of Ag_3PO_4 has been successfully created using the coprecipitation and chemisorption method. The first step is the coprecipitation of Ag_3PO_4 under ethanol-water solution using the material of $AgNO_3$ and $Na_2HPO_4.12H_2O$, and the second step is the chemisorption of $AuCl_4^-$ ion on Ag_3PO_4 under sonication. This design aims to improve the photocatalytic activity of Ag_3PO_4 through an Au and $AuCl_4^-$. Incorporation of these species on the Ag_3PO_4 surface can increase the electron capture and prevent photogenerated electron-hole recombination, leading to high photocatalytic activity.

2. Materials and Methods

2.1 Synthesis of Photocatalysts

The chemicals of $AgNO_3$ (ACS, ISO, Reag. Ph Eur; Merck), $Na_2HPO_4.12H_2O$ (ISO, Reag. Ph Eur, Merck), $HAuCl_4.4H_2O$ (purity: 99.9%, Shandong Honrel Co. Ltd), and ethanol (absolute for analysis, Merck), were used for the synthesis of samples. The samples of APO (Ag_3PO_4) and E-APO (Ag_3PO_4 prepared under ethanol solution) were synthesized using the coprecipitation method [22,23]. To prepare the E-APO sample, the $AgNO_3$ (0.85 g) was dissolved in 200 mL of ethanol solution (50% of ethanol in water). The Na_2HPO_4 solution was prepared by dissolving 1.8 g of $Na_2HPO_4.12H_2O$ in 50 mL of deionized water. $AgNO_3$ in ethanol solution was slowly added (dropwise) by Na_2HPO_4 solution. The precipitate of E-APO was filtered and washed with deionized water and subsequently dried in an oven at 60 °C for 4 h. The sample of APO as control was synthesized with a similar procedure but without ethanol. The APO/Au (Au in Ag_3PO_4) and E-APO/Au (Au in Ag_3PO_4 prepared under ethanol solution) were synthesized using the chemisorption method. Firstly, the Au solutions were prepared using $HAuCl_4.4H_2O$ dissolved in water with a concentration of 1 mg/mL. The 0.5 gram of APO and E-APO powder were each mixed with 10 mL of water to obtain the suspension. The Au solu-

tions (10 mL) were added to the suspension and sonicated for 15 minutes. The products were filtered and washed with water and dried in an oven at 60 °C for 4 h.

2.2 Catalysts Characterizations

All samples were characterized using X-ray diffraction (XRD, Bruker D2 Phaser) with Cu Kα radiation, λ=1.5418 Å. Absorption spectra were measured using diffuse reflectance spectroscopy (DRS, JASCO V-670). Morphology and particle size of E-APO/Au were investigated using SEM. The binding energies of Ag3d, P2p, O1s, and Au4f of E-APO/Au were investigated using XPS (ULVAC PHI 5600, ULVAC PHI Co., Ltd), calibrated by internal reference of the adventitious carbon.

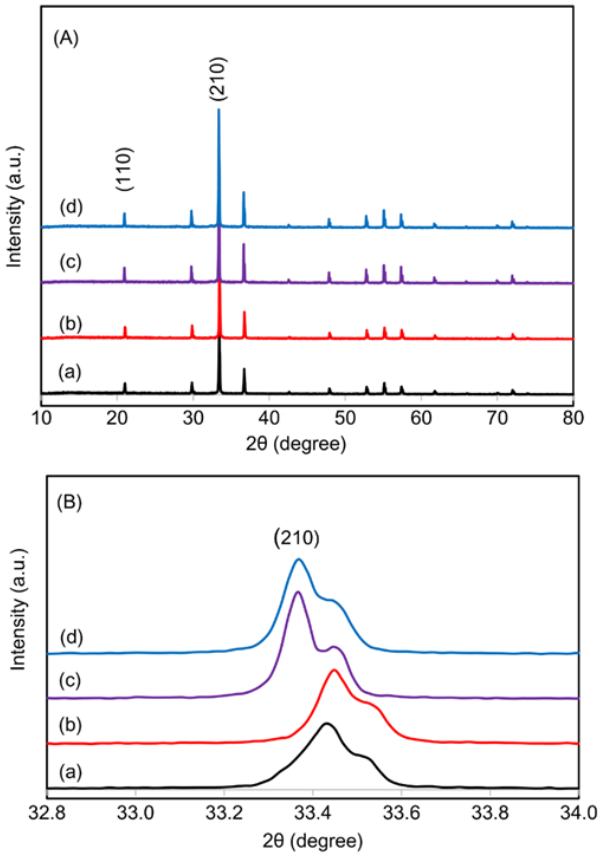

Figure 1. (A) XRD profile of APO (a), E-APO (b), APO/Au (c), E-APO/Au (d), and (B) their shifts of (210) Miller indices.

2.3 Photocatalytic Activities

The photocatalytic activities were evaluated under visible light irradiation (Ranpo, LED Spotlight 3 W, blue light) [23]. The catalysts of 0.1 g were added to 100 mL of RhB solution (10 mg/L) then equilibrated for 20 minutes. The sample of RhB solution (5 mL) was withdrawn and centrifuged at 5000 rpm to separate the solution from the catalyst and the concentration was measured using the spectrophotometer. The mechanism of photocatalyst in the surface of E-APO/Au was investigated using benzoquinone (BQ), ammonium oxalate (AO), and isopropyl alcohol (IPA) as a scavenger of $O_2^{\bullet -}$, h^+, and $^{\bullet}OH$, respectively [22].

3. Results and discussion

3.1 Characterization of Photocatalysts

The structure of photocatalysts was investigated using the XRD and the results are displayed in Figure 1A. All samples showed a similar structure of body-centered cubic Ag_3PO_4 (JCPDS no.06-0505) [24]. Due to a very small concentration of Au, the (111) plane of Au was not observed in the XRD. The doublet peak was observed at (210) plane at the highest peak (2θ) of 33.4074°, 33.4479°, 33.3668°, 33.3668° for APO, E-APO, APO/Au, and E-APO/Au, respectively (Figure 1B). The shift of (210) peaks was observed after incorporating the Au into the Ag_3PO_4. Both APO/Au and E-APO/Au exhibited a lower 2θ compared to the Au-untreated photocatalysts. The *d*-space (Å) of the (210) plane can be measured from the XRD data, resulting in 2.6821, 2.6790, 2.6853, and 2.6853 for APO, E-APO, APO/Au, and E-APO/Au, respectively. The d-space of E-APO is slightly lower than APO, indicating that the preparation with ethanol-water might form a silver vacancy. The changed polarity of solvent can affect the coprecipitation of Ag_3PO_4 leading

Table 1. The characterization of Ag_3PO_4 synthesized under different preparation.

Samples	Preparation	Peaks of (210) (2θ)	*d*-space of (210) plane (Å)	The intensity ratio of (210)/(110)	Bandgap energy (eV)
APO	water	33.4074	2.6821	7.2	2.40
E-APO	ethanol-water	33.4479	2.6790	7.6	2.37
APO/Au	water, $HAuCl_4.4H_2O$	33.3668	2.6853	8.4	2.42
E-APO/Au	ethanol-water, $HAuCl_4.4H_2O$	33.3668	2.6853	8.0	2.42

to a defect formation of silver vacancy. This phenomenon can lead to a shrinkage of the lattice. In contrast, incorporating Au on the Ag_3PO_4 slightly increases the d-space, indicating that the Au was successfully incorporated in Ag_3PO_4 leading to the expansion of the lattice.

The (210)/(110) intensity ratio of 7.2, 7.6, 8.4, 8.0 can be found in the samples of APO, E-APO, APO/Au, and E-APO/Au, respectively. The Au-treated samples showed a higher intensity ratio of (210)/(110) plane, indicating that the incorporation of Au might change the plane atomic composition of the crystal. The XRD data of Ag_3PO_4 prepared under different treatments can be summarized in Table 1. The morphology of E-APO/Au was also investigated under SEM, showing that a spherical and irregular shape with the particle size distribution of 100-400 nm was created (Figure 2).

To investigating the effect of different preparation, the spectra absorptions of APO, E-APO, APO/Au, and E-APO/Au are scanned and the results are displayed in Figure 3. The absorption of E-APO along the visible region has higher than that of APO, indicating the defect of silver vacancy might be generated in E-APO that is consistent with the previous result [22]. The incorporating Au in both APO/Au and E-APO/Au generated a broad absorption peak at 520 to 640 nm (insert picture of Figure 3). These absorptions might originate from the surface plasmon resonance of Au metallic nanocluster in Ag_3PO_4 [25]. Due to the small amount of metallic Au on the surface of Ag_3PO_4, these plasmon absorptions are not so strong.

The optical bandgap of the samples can be estimated using Tauc's relation [26] using the following Equation (1):

$$\alpha h\nu = A\left(h\nu - E_g\right)^n \quad (1)$$

where, α is the absorption coefficient, h is Planck's constant, ν is the transition frequency, A is a constant, E_g is the bandgap energy, and the exponent n represents the nature of transitions. The bandgap energy is determined from the linear extrapolation of $(\alpha h\nu)^2$ versus $h\nu$ (n=1/2 for direct allowed transition). The results showed that the optical bandgap energies of APO, E-APO, APO/Au, and E-APO/Au are 2.40 eV, 2.37 eV, 2.42 eV, 2.42 eV respectively (Table 1). The decrease of bandgap in the E-APO sample might be caused by the defect of silver vacancy [22], whereas the increase of bandgap in APO/Au and E-APO/Au might be caused by Au incorporation on the surface.

The XPS profile of the Ag_3PO_4 (E-APO/Au) was displayed in Figure 4. The peak of 373.9 and 367.9 eV originates from the $Ag3d_{3/2}$ and $Ag3d_{5/2}$ respectively, indicating that the state of silver is Ag^+ (Figure 4a) and no Ag metallic was formed [27]. The $P2p_{1/2}$ and $P2p_{3/2}$ were also observed at 133.4 eV and 132.4 eV, indicating that the P^{+5} existed in the surface of Ag_3PO_4 (Figure 4b) [28]. There are two types of oxygen at 532.2. eV and 530.5 eV which are assigned to the oxygen of hydroxyl in the surface and oxygen in the lattice, respectively (Figure 4c) [29]. The Au incorporation was observed in XPS spectra with an atomic percent of 3.34% (2.12% metal Au^0 and 1.22% ion Au^{3+}). There are two states of Au in the samples suggesting that both metallic and ionic were formed in the surface as shown in Figure 4d. The 88.4 eV and 84.7 eV originate from the $Au4f_{5/2}$ and $Au4f_{7/2}$ respectively with a spin–orbital doublet split-

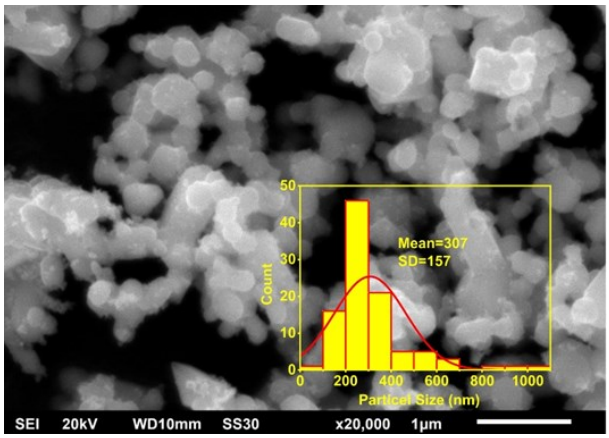

Figure 2. SEM image of E-APO/Au (Ag_3PO_4 synthesized using coprecipitation method under ethanol solution and chemisorption method under $AuCl_4^-$ solution).

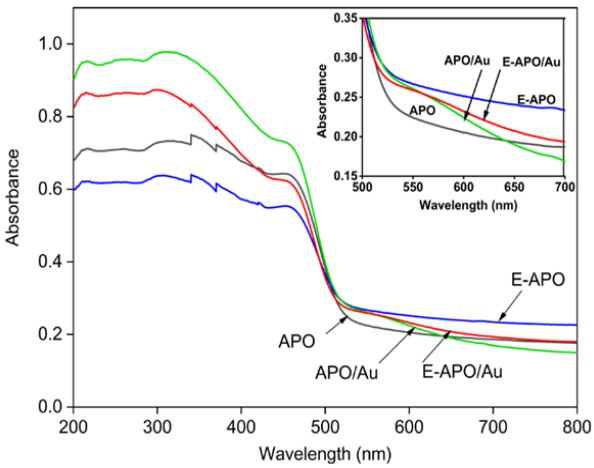

Figure 3. The DRS absorption of APO, E-APO, APO/Au, and E-APO/Au.

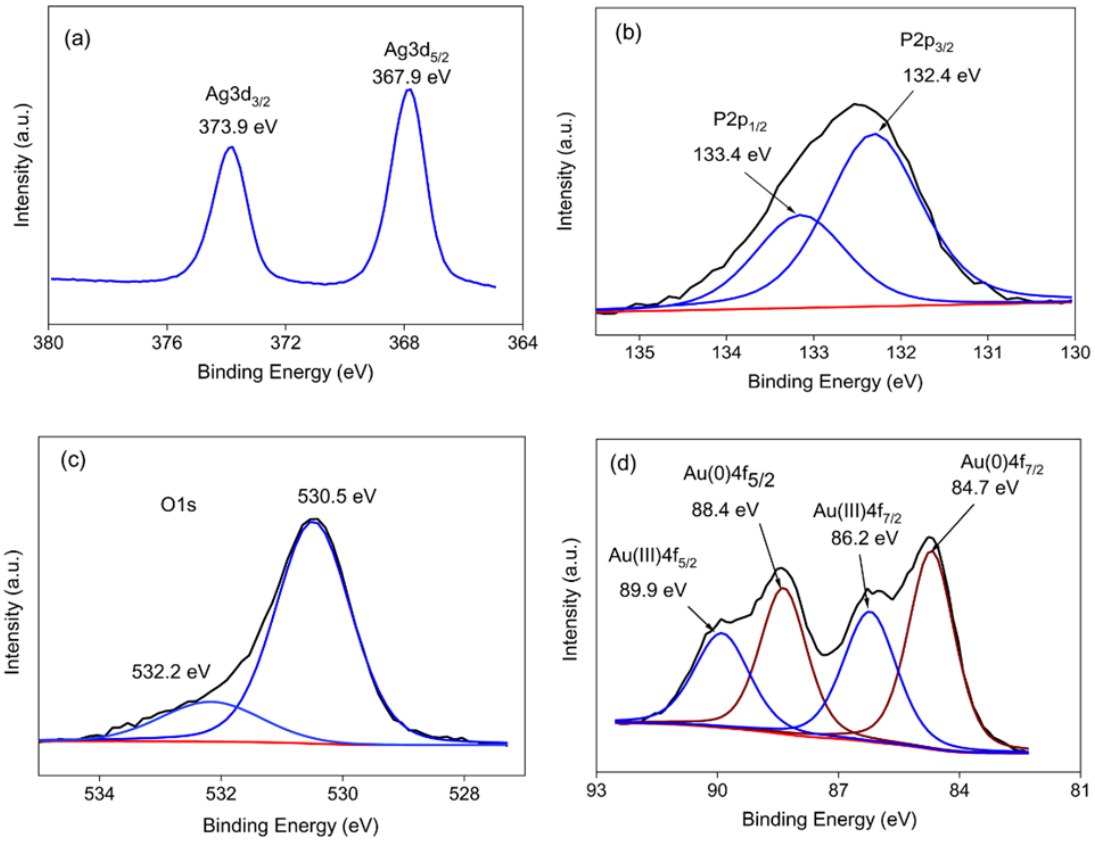

Figure 4. The XPS profile of E-APO/Au photocatalyst: Ag3d (a), P2p (b), O1s (c), and Au4f (d).

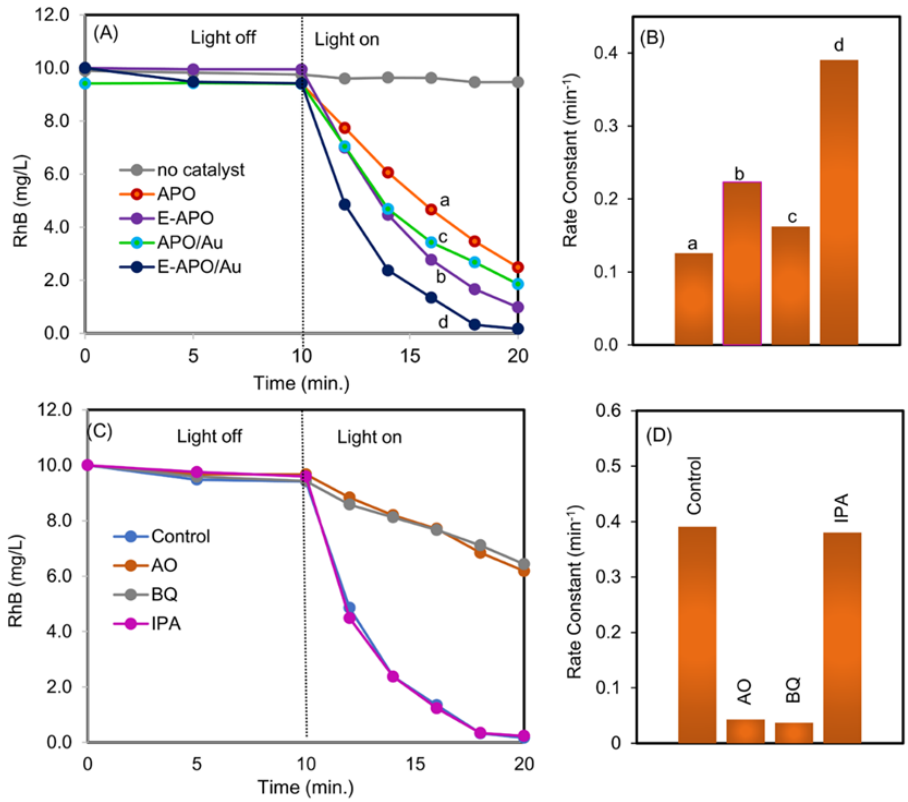

Figure 5. (A) Photocatalytic activity of APO (a), E-APO (b), APO/Au (c), and E-APO/Au (d) with (B) their rate constants and (C) the investigation of reaction mechanism on E-APO/Au using the ammonium oxalate (AO), benzoquinone (BQ), and isopropyl alcohol (IPA) as a scavenger with (D) their rate constants.

ting of 3.7 eV that confirms the existence of Au^0 states [27]. Whereas, the Au^{3+} found at 89.9 eV and 86.2 eV came from the $Au4f_{5/2}$ and $Au4f_{7/2}$, respectively [30].

An impressive result was found in the calculation of the Ag/P atomic ratio from the XPS data. The Ag/P atomic ratio of 3.76 was observed in E-APO/Au. This value was higher compared to the Ag_3PO_4 (2.80) and defect-Ag_3PO_4 (2.49) that were previously reported [23]. The high ratio of Ag/P suggesting that the phosphate was substituted by Au and $AuCl_4^-$. Interestingly, the atomic ratio of Ag/P in E-APO/Au was higher than the incorporating platinum complexes on the defect-Ag_3PO_4 (2.97) [23]. This higher ratio of Ag/P in E-APO/Au might be induced by metallic Au formation on the lattice of Ag_3PO_4 which replaced much higher phosphate ion. Therefore, phosphate deficiency in E-APO/Au was created.

Based on XPS analysis, the formation of $AuCl_4^-$ and Au^0 can be explained. The compound of $HAuCl_4.4H_2O$ can be ionized into $AuCl_4^-$ ions in water. $AuCl_4^-$ ions can substitute PO_4^{3-} ions of Ag_3PO_4 on the surface. This unbalanced charge species substitution might easily induce electron transfers. During this process, the photoreduction of $AuCl_4^-$ in low intensity of lightroom might occur, resulting in Au^0. Therefore, both $AuCl_4^-$ and Au^0 existed on the surface of Ag_3PO_4 as observed in XPS.

3.2 Photocatalytic Evaluation

Figure 5A showed the photocatalytic activity of APO, E-APO, APO/Au, and E-APO/Au. The photocatalytic activity rates are studied using the pseudo-first-order kinetics, $\ln(C_0/C_t)=kt$, where C_0 and C_t are the RhB concentration at times 0 and t, respectively, and k is the rate constant [22]. After plotting $\ln(C_0/C_t)$ versus t, all reactions followed the pseudo-first-order kinetics with the rate constant of 0.126 min^{-1}, 0.223 min^{-1}, 0.162 min^{-1}, and 0.391 min^{-1} for the samples of APO, E-APO, APO/Au, and E-APO/Au, respectively (Figure 5B). The ethanol treatment in the preparation of samples enhances catalytic activities. The incorporation of Au on APO increases the catalytic activity as found in the APO/Au sample however it is lower than the E-APO sample. The lower activity might be caused by the lower absorption of APO/Au in the visible region due to decreased amount of electron excitation on the surface. The treatment of Au on E-APO significantly improves the photocatalytic activity as found in E-APO/Au. It was increased 3 times higher compared to the APO. The highest activity of E-APO/Au might be caused by the dual effect of Au^0 and $AuCl_4^-$ that acted as effective electron acceptors on the surface of Ag_3PO_4.

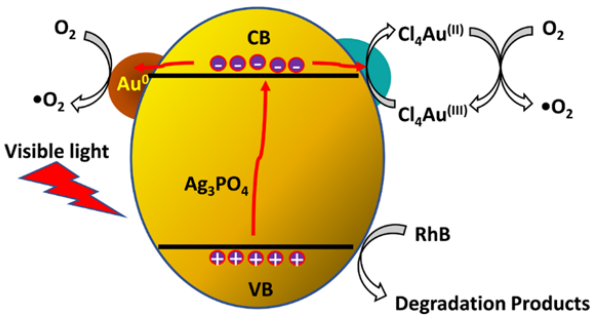

Figure 6. Proposed mechanism of photocatalytic reaction on the surface of E-APO/Au.

The photocatalytic reaction mechanism in E-APO/Au surface was studied using ammonium oxalate (AO), benzoquinone (BQ), and isopropyl alcohol (IPA) as a scavenger for the hole (h^+), superoxide radicals ($O_2^{\bullet -}$), and hydroxyl radical ($^\bullet OH$), respectively [31]. The mechanism of these scavengers can be summarized by reaction (2–4) based on literature reports [32–34].

$$C_6H_4O_2 + O_2^{\bullet -} \rightarrow C_6H_4O_2^{\bullet -} + O_2 \text{ (BQ)} \quad (2)$$

$$C_2O_4^{2-} + h^+ \rightarrow CO_2^{\bullet -} + CO_2 \text{ (AO)} \quad (3)$$

$$CH_3CHOHCH_3 + {}^\bullet OH \rightarrow CH_3{}^\bullet COHCH_3 + H_2O \text{ (IPA)} \quad (4)$$

The results of the reaction mechanism study were shown in Figures 5C and 5D. The reactions in the surface were suppressed under the addition of AO and BQ, indicating that the role of hole and superoxide radicals were more prominent in the reaction. Based on this investigation, the reaction mechanism can be summarized in reactions (5–13).

$$Ag_3PO_4 + h\nu \rightarrow h^+_{(vb)} + e^-_{(cb)} \quad (5)$$

$$e^-_{(cb)} \rightarrow e^-_{(>Au)} \quad (6)$$

$$e^-_{(cb)} + >Au^{(II)}Cl_4^- \rightarrow >Au^{(II)}Cl_4^{2-} \quad (7)$$

$$>Au^{(II)}Cl_4^{2-} + O_2 \rightarrow >Au^{(III)}Cl_4^- + O_2^{\bullet -} \quad (8)$$

$$O_2 + e^-_{(>Au)} \rightarrow O_2^{\bullet -} \quad (9)$$

$$O_2^{\bullet -} + e^-_{(>Au/cb)} + 2H^+ \rightarrow H_2O_2 \quad (10)$$

$$O_2^{\bullet -} + H_2O_2 \rightarrow {}^\bullet OH + OH^- + O_2 \quad (11)$$

$$h^+ + H_2O \rightarrow {}^\bullet OH + H^+ \quad (12)$$

$$^\bullet OH + RhB \rightarrow CO_2 + H_2O + NO_3^- + NH_4^+ \quad (13)$$

The proposed mechanism in the surface of E-APO/Au can be illustrated and shown in Figure 6. Under visible light irradiation, the photo-excited electrons are injected into the conduction band of Ag_3PO_4. At the same time, the Au(III) ion acts as an electron acceptor and carries out the redox reaction on the surface of the photocatalyst, producing superoxide radicals.

Meanwhile, the metallic Au incorporated on the surface of Ag_3PO_4 generated the highest Schottky barrier that also facilitated the electron transfer [10]. The trapped electron is transferred to the adsorbed oxygen, producing superoxide radicals. These phenomena promote charge separation leading to high photocatalytic activity. The excellent photocatalytic activity is ascribed to efficient electron transfer from the conduction band of Ag_3PO_4 to Au(III) complexes chemically bonded surface and metallic Au, which brings to high charge separation, resulting in higher quantities of $O_2^{\bullet -}$ radical anions [35]. The $O_2^{\bullet -}$ radical anions under excess electron can produce H_2O_2, resulting in much higher $^{\bullet}OH$ radicals. These species have very important roles in the oxidation of RhB into CO_2, H_2O, NO_3^-, and NH_4^+ [36].

4. Conclusions

The metallic Au nanoparticles and $AuCl_4^-$ complexes ions were successfully incorporated on the surface of Ag_3PO_4. The ion of $AuCl_4^-$ complex substituted the PO_4^{3-} of Ag_3PO_4 surface. The substitution was effectively on Ag_3PO_4 that synthesized under ethanol-water solution. The high photocatalytic activity of $Au/AuCl_4^-$ Ag_3PO_4 was mainly caused by metallic Au and Au(III) complex as electron acceptors.

Acknowledgment

This research was supported by the Directorate of Research and Community Service, Deputy of Strengthening Research and Development, Ministry of Research and Technology/National Research and Innovation Agency, Number: 176/SP2H/AMD/LT/DRPM/2020.

References

[1] Wibowo, D., Muzakkar, M.Z., Saad, S.K.M., Mustapa, F., Maulidiyah, M., Nurdin, M., Umar, A.A. (2020). Enhanced visible light-driven photocatalytic degradation supported by Au-TiO_2 coral-needle nanoparticles. *Journal of Photochemistry and Photobiology A: Chemistry*, 398, 112589. DOI: 10.1016/j.jphotochem.2020.112589

[2] Duan, Z., Huang, Y., Zhang, D., Chen, S. (2019). Electrospinning Fabricating Au/TiO_2 network-like nanofibers as visible light activated photocatalyst. *Scientific Reports*, 9, 8008. DOI: 10.1038/s41598-019-44422-w

[3] Shoeir, K., Kandil, S., El-hosainy, H., El-Kemary, M. (2019). Tailoring the surface reactivity of plasmonic Au@TiO_2 photocatalyst bio-based chitosan fiber towards cleaner of harmful water pollutants under visible-light irradiation. *Journal of Cleaner Production*, 230, 383–393. DOI: 10.1016/j.jclepro.2019.05.103

[4] Campagnolo, L., Lauciello, S., Athanassiou, A., Fragouli, D. (2019). Au/ZnO hybrid nanostructures on electrospun polymeric mats for improved photocatalytic degradation of organic pollutants. *Water*, 11(9), 1787. DOI: 10.3390/w11091787

[5] Kavitha, R., Kumar, S.G. (2019). A review on plasmonic Au-ZnO heterojunction photocatalysts: Preparation, modifications and related charge carrier dynamics. *Materials Science in Semiconductor Processing*, 93, 59–91. DOI: 10.1016/j.mssp.2018.12.026

[6] He, C., Li, X., Li, Y., Li, J., Xi, G. (2017). Large-scale synthesis of Au–WO_3 porous hollow spheres and their photocatalytic properties. *Catalysis Science & Technology*, 7, 3702–3706. DOI: 10.1039/C7CY01399J

[7] Xian, T., Di, L., Sun, X., Ma, J., Zhou, Y., Wei, X. (2018). Photocatalytic degradation of dyes over Au decorated $SrTiO_3$ nanoparticles under simulated sunlight and visible light irradiation. *Journal of the Ceramic Society*, 126(5), 354–359. DOI: 10.2109/jcersj2.17244

[8] Nguyen, C.C., Sakar, M., Vu, M.H., Do, T.O. (2019). Nitrogen vacancies-assisted enhanced plasmonic photoactivities of Au/g-C_3N_4 crumpled nanolayers: A novel pathway toward efficient solar light-driven photocatalysts. *Industrial & Engineering Chemistry Research*, 58(9), 3698–3706. DOI: 10.1021/acs.iecr.8b05792

[9] Wang, L., Chong, J., Fu, Y., Li, R., Liu, J., Huang, M. (2020). A novel strategy for the design of Au@CdS yolk-shell nanostructures and their photocatalytic properties. *Journal of Alloys and Compounds*, 834, 155051. DOI: 10.1016/j.jallcom.2020.155051

[10] Li, X. Z., Li, F.B. (2001). Study of Au/Au^{3+}-TiO_2 photocatalysts toward visible photooxidation for water and wastewater treatment. *Environmental Science & Technology*, 35(11), 2381–2387. DOI: 10.1021/es001752w

[11] Ye, Y., Wang, K., Huang, X., Lei, R., Zhao, Y., Liu, P. (2019). Integration of piezoelectric effect into a Au/ZnO photocatalyst for efficient charge separation. *Catalysis Science & Technology*, 9, 3771–3778. DOI: 10.1039/C9CY00920E.

[12] Khan, M.R., Chuan, T.W., Yousuf, A., Chowdhurya, M.N.K., Cheng, C.K. (2015). Schottky barrier and surface plasmonic resonance phenomena towards the photocatalytic reaction: Study of their mechanisms to enhance photocatalytic activity. Catalysis Science and Technology, 5, 2522–2531. DOI: 10.1039/C4CY01545B

[13] Jia, Y., Ma, H., Liu, C. (2019). Au nanoparticles enhanced Z-scheme Au-$CoFe_2O_4$/MoS_2 visible light photocatalyst with magnetic retrievability. *Applied Surface Science*, 463, 854–862. DOI: 10.1016/j.apsusc.2018.09.008

[14] Zhang, G., Zhu, X., Chen, D., Li, N., Xu, Q., Li, H., He, J., Xu, H., Lu, J. (2020). Hierarchical Z-scheme g-C_3N_4/Au/$ZnIn_2S_4$ photocatalyst for highly enhanced visible-light photocatalytic nitric oxide removal and carbon dioxide conversion. *Environmental Science: Nano*, 7, 676–687. DOI: 10.1039/C9EN01325C

[15] Shin, J., Heo, J.N., Do, J.Y., Kim, Y.I., Yoon, S.J., Kim, Y.S., Kang, M. (2020). Effective charge separation in rGO/$NiWO_4$@Au photocatalyst for efficient CO_2 reduction under visible light. *Journal of Industrial and Engineering Chemistry*, 81, 427–439. DOI: 10.1016/j.jiec.2019.09.033

[16] Hu, G., Hu, C.X., Zhu, Z.Y., Zhang, L., Wang, Q., Zhang, H.L. (2018). Construction of Au/CuO/Co_3O_4 tricomponent heterojunction nanotubes for enhanced photocatalytic oxygen evolution under visible light irradiation. *ACS Sustainable Chemistry & Engineering*, 6(7), 8801–8808. DOI: 10.1021/acssuschemeng.8b01153

[17] Zhang, W., Li, G., Liu, H., Chen, J., Ma, S., An, T. (2019). Micro/nano-bubble assisted synthesis of Au/TiO_2@CNTs composite photocatalyst for photocatalytic degradation of gaseous styrene and its enhanced catalytic mechanism. *Environmental Science: Nano*, 6, 948–958 (2019). DOI: 10.1039/C8EN01375F.

[18] Yi, Z., Ye, J., Kikugawa, N., Kako, T., Ouyang, S., Stuart-Williams, H., Yang, H., Cao, J., Luo, W., Li, Z., Liu, Y., Withers, R.L. (2010). An orthophosphate semiconductor with photooxidation properties under visible-light irradiation. *Nature Materials*, 9, 559–564. DOI: 10.1038/nmat2780

[19] Yan, T., Zhang, H., Liu, Y., Guan, W., Long, J., Li, W., You, J. (2014). Fabrication of robust M/Ag_3PO_4 (M = Pt, Pd, Au) Schottky-type heterostructures for improved visible-light photocatalysis. *RSC Advances*, 4, 37220–37230. DOI: 10.1039/C4RA06254J

[20] Wang, F.R., Wang, J.D., Sun, H.P., Liu, J.K., Yang, X.H. (2017). Plasmon-enhanced instantaneous photocatalytic activity of Au@Ag_3PO_4 heterostructure targeted at emergency treatment of environmental pollution. *Journal of Materials Science*, 52, 2495–2510. DOI: 10.1007/s10853-016-0544-x

[21] Liu, C.F., Perng, T.P. (2020). Fabrication and band structure of Ag_3PO_4–TiO_2 heterojunction with enhanced photocatalytic hydrogen evolution. *International Journal of Hydrogen Energy*, 45(1), 149–159. DOI: 10.1016/j.ijhydene.2019.10.182

[22] Sulaeman, U., Hermawan, D., Andreas, R., Abdullah, A.Z., Yin, S. (2018). Native defects in silver orthophosphate and their effects on photocatalytic activity under visible light irradiation. *Applied Surface Science*, 428, 1029–1035. DOI: 10.1016/j.apsusc.2017.09.188

[23] Sulaeman, U., Permadi, R.D., Ningsih, D.R., Diastuti, H., Riapanitra, A., Yin, S. (2020). The surface modification of Ag_3PO_4 using anionic platinum complexes for enhanced visible-light photocatalytic activity. *Materials Letters*, 259, 126848. DOI: 10.1016/j.matlet.2019.126848

[24] Qin, Y., Li, F., Tu, P., Ma, Y., Chen, W., Shi, F., Xiang, Q., Shan, H., Zhang, L., Tao, P., Song, C., Shang, W., Deng, T., Zhu, H., Wu, J. (2018). Ag_3PO_4 electrocatalyst for oxygen reduction reaction: enhancement from positive charge. *RSC Advances*, 8, 5382–5387. DOI: 10.1039/C7RA12643C

[25] Tanaka, A., Ogino, A., Iwaki, M., Hashimoto, K., Ohnuma, A., Amano, F., Ohtani, B., Kominami, H. 2012. Gold–titanium(IV) oxide plasmonic photocatalysts prepared by a colloid-photodeposition method: correlation between physical properties and photocatalytic activities. *Langmuir*, 28(36), 13105–13111. DOI: 10.1021/la301944b

[26] Mishra, M., Kuppusami, P., Sairam, T.N., Singh, A., Mohandas, E. (2011). Effect of substrate temperature and oxygen partial pressure on microstructure and optical properties of pulsed laser deposited yttrium oxide thin films. *Applied Surface Science*, 257, 7665–7670. DOI: 10.1016/j.apsusc.2011.03.156

[27] Liu, Z., Liu, Y., Xu, P., Ma, Z., Wang, J., Yuan, H. (2017). Rational Design of Wide Spectral-Responsive Heterostructures of Au Nanorod Coupled Ag_3PO_4 with Enhanced Photocatalytic Performance. *ACS Applied Materials & Interfaces*, 9(24), 20620–20629. DOI: 10.1021/acsami.7b06824

[28] Xie, Q., Li, Y., Lv, Z., Zhou, H., Yang, X., Chen, J., Guo, H. (2017). Effective Adsorption and Removal of Phosphate from Aqueous Solutions and Eutrophic Water by Fe-based MOFs of MIL-101, *Scientific Reports*, 7, 3316. DOI: 10.1038/s41598-017-03526-x

[29] Chong, R., Cheng, X., Wang, B., Li, D., Chang, Z., Zhang, L. (2016). Enhanced photocatalytic activity of Ag_3PO_4 for oxygen evolution and Methylene blue degeneration: Effect of calcination temperature. *International Journal of Hydrogen Energy*, 41, 2575−2582. DOI: 10.1016/j.ijhydene.2015.12.061

[30] Sylvestre, J.-P., Poulin, S., Kabashin, A.V., Sacher, E., Meunier, M., Luong, J.H.T. (2004). Surface Chemistry of Gold Nanoparticles Produced by Laser Ablation in Aqueous Media. *Journal of Physical Chemistry B*, 108 (43), 16864−16869. DOI: 10.1021/jp047134+

[31] Li, S., Hu, S., Jiang, W., Liu, Y., Liu, J., Wang, Z. (2017). Synthesis of n-type TaON microspheres decorated by p-type Ag_2O with enhanced visible light photocatalytic activity. *Molecular Catalysis*, 435, 135–143. DOI: 10.1016/j.mcat.2017.03.027

[32] Zhu, M., Lu, J., Hu, Y., Liu, Y., Hu, S., Zhu, C. (2020). Photochemical reactions between 1,4-benzoquinone and $O_2^{\bullet-}$. *Environmental Science and Pollution Research*, 27, 31289–31299. DOI: 10.1007/s11356-020-09422-8

[33] Forouzan, F., Thomas C. Richards, T.C., Bard, A.J. (1996). Photoinduced reaction at TiO_2 particles. Photodeposition from Ni^{II} solutions with oxalate, *Journal of Physical Chemistry*, 100, 18123–18127. DOI: 10.1021/jp953241f

[34] Flyunt, R., Knolle, W., Kahnt, A., Halbig, C. E., Lotnyk, A., Häupl, T., Prager, A., Eigler, S., Abel, B. (2016). High quality reduced graphene oxide flakes by fast kinetically controlled and clean indirect UV-induced radical reduction. *Nanoscale*, 8, 7572–7579. DOI: 10.1039/C6NR00156D.

[35] Zhao, W., Chen, C., Ma, W., Zhao, J., Wang, D., Hidaka, H., Serpone, N. (2003). Efficient Photoinduced Conversion of an Azo Dye on Hexachloroplatinate(III)-Modified TiO_2 Surfaces under Visible Light Irradiation–A Photosensitization Pathway. *Chemistry–A European Journal*, 9, 3292–3299. DOI: 10.1002/chem.200204559

[36] Kavinkumar, V., Jaihindh, D.P., Verma, A., Jothivenkatachalam, K., Fu, Y. (2019). Influence of cobalt substitution on the crystal structure, band edges and photocatalytic property of hierarchical Bi_2WO_6 microsphere. *New Journal of Chemistry*, 43, 9170–9182. DOI: 10.1039/C9NJ00170K.